Combinatorial DNA damage pairing model based on X-ray-induced foci predicts the dose and LET dependence of cell death in human breast cells

Nikhil Vadhavkar[1], Christopher Pham[2], Walter Georgescu[3], Thomas Deschamps[3], Anne-Catherine Heuskin[4], Jonathan Tang[3], and Sylvain V. Costes[3*]

1. MIT Man-Vehicle Laboratory, Massachusetts Institute of Technology, 77 Massachusetts Avenue, Cambridge MA 02139

2. Department of Radiation Physics, University of Texas M.D. Anderson Cancer Center

3. Life Sciences Division, Lawrence Berkeley National Laboratory, MS:977, Berkeley, CA 94720

4. Namur Research Institute for Life Sciences (NARILIS), Research Center for the Physics of Matter and Radiation (PMR), University of Namur, Belgium

* To whom the correspondence should be addressed: svcostes@lbl.gov

Corresponding Author: Sylvain Costes

Pages: 17

Figures: 4

Key Words: radiation risk modeling, DNA double-strand breaks, radiation-induced foci, relative biological effectiveness, cancer risk

Abbreviations:

DSB: Double-strand break

HMEC: Human mammary epithelial cells

IR: Ionizing radiation

HZE: High atomic number and energy

LET: Linear energy transfer (typical unit: keV/µm)

Post-IR: Following exposure to ionizing radiation

RIF: Radiation-induced foci

RMSE: Root-mean-square error

ABSTRACT

In contrast to the classic view of static DNA double strand breaks (DSBs) being repaired at the site of damage, we hypothesize that DSBs move and merge with each other over large distances (μm). As X-ray dose increases, the probability of having DSB clusters increases and so does the probability of misrepair and cell death. Experimental work characterizing the dose dependence of radiation-induced foci (RIF) from X-ray in nonmalignant human mammary epithelial cells (MCF10A) is used here to validate a DSB clustering model. We then use the principles of the local effect model (LEM) to predict the yield of DSB at the sub-micron level. Two mechanisms for DSB clustering are first compared: random coalescence of DSBs versus active movement of DSBs into repair domains. Simulations that best predict both RIF dose dependence and cell survival following X-ray favor the repair domain hypothesis, suggesting the nucleus is divided into an array of regularly spaced repair domains of ~1.55 μm sides. Applying the same approach to high-LET ion tracks, we can predict experimental RIF/μm along tracks with an overall relative error of 12%, for LET ranging between 30 and 350 keV/μm and for three different ions. Finally, cell death is predicted by assuming an exponential dependence on the total number of DSBs and of all possible combinations of paired DSBs within each simulated RIF. RBE predictions for cell survival of MCF10A exposed to high-LET show an LET dependence that matches previous experimental results for similar cell types. Overall, this work suggests that microdosimetric properties of ion tracks at the sub-micron level are sufficient to explain both RIF data and survival curves for any LET, similarly to the LEM assumption. On the other hand, high-LET death mechanism does not have to infer linear-quadratic dose formalism as done in the LEM. In addition, the size of repair domains derived in our model are based on experimental RIF and are three times larger than the hypothetical LEM voxel used to fit survival curves. Our model is therefore an alternative to previous approaches by providing a testable biological mechanism (i.e. RIF). More generally, DSB pairing will help develop more accurate alternatives to the simplistic linear cancer risk model (LNT) currently used for regulating exposure to very low levels of ionizing radiation.

INTRODUCTION

Space programs are currently shifting focus to exploration outside of low Earth orbit, in particular long-duration missions to the moon and Mars. However, the continuous exposure of astronauts to galactic cosmic rays (GCR) is one of the main concerns for long-term missions [1]. The GCR spectrum contains a large component of high-LET particles, such as He ions and heavier ions such as carbon and iron (HZE particles, i.e. particles with high charge and energy). Risk uncertainties for space radiation tumorigenesis are typically inferred from low-LET risk using a quality factor or RBE (relative biological effectiveness) [2]. RBE as high as 40 have been reported for Harderian gland tumors detected in mice exposed to 600 MeV/n Fe [3]. In other words, it takes 40 times more dose of X-rays to lead to the same tumor incidence than with HZE Fe. In contrast, in vitro studies for mammalian cell survival have led to much lower RBE with values ~2 for primary human breast epithelial cell survival exposed to 1 GeV/n Fe [4] or between 2 to 10 for chromosomal aberrations for various HZE [5]. There are therefore discrepancies between in vitro and in vivo responses, and mechanistic models may help resolve such discrepancies.

RBE greater than unity is thought to reflect the fact that DNA lesions induced by HZE are more complex [6]. However a unified formalism able to model DNA complexity in a way that can predict cell survival for various radiation qualities remains to be accepted [7]. Therefore, RBE is often measured for each cell, particle and energy of interest. Survival curves are typically fitted with a linear quadratic model introduced by Douglas and Fowler [8] for both the radiation reference (X-ray) and the particle of interest, and RBE is computed as the ratio between the dose inducing 10% survival with X-ray over the dose inducing the same survival with HZE.

In this work, we present a formalism inspired from the Local Effect Model (LEM), which assumes DNA damage and cell death can be solely predicted by the amount of energy deposited in a small sub-nuclear volume, independently of the radiation quality [9]. With such an approach, one can predict survival curves for any HZE based on biological properties derived from X-ray data alone. This work completes the LEM in two ways: 1. Radiation Induced Foci (RIF) dependence on dose, LET and spatial distribution is reported here for human breast cells and used to develop a model mimicking DSB clustering mechanisms. 2. Probability of cell death does not assume a linear quadratic dependence with dose and instead uses probabilities based on the number of combinations of DSB pairs in each DSB cluster.

RESULTS

Experimental setup to characterize RIF distribution along HZE tracks.

We measure DNA damage induced by ionizing radiation (IR) by quantifying microscopically visible nuclear domains (i.e. foci) marked by recruitment of p53 Binding protein 1 (53BP1). We have previously shown that X-ray elicits radiation-induced foci (RIF) that are sparsely distributed in the nucleus [10]. In contrast, HZE irradiation leads to streaks of RIF that can be observed through the cell nucleus along the trajectory of a particle. To visualize these tracks, cells were compartmentalized into eight well chamber

slides (Fig. 1A) and exposed to a beam of HZE parallel to the two slides. Entry energy for the beam was chosen so that the ion would stop in the last well of the second chamber (8^{th} well after going through 8 cm of water/plastic). By precisely keeping track of the position on a motorized stage mounted on our microscope, we could derive the energy and LET of the ion as a function of position (Graph in Fig. 1A). This was derived by computing the stopping power of water and the range of ions in water using the software SRIM[11] (www.srim.org). The validity of our approach was confirmed by computing the amount of γH2AX RIF signal as a function of stage, which showed that the amount of DNA damage dropped significantly at the expected location in the slide (Fig. 1B,C). Individual HZE track detection within each nucleus was done as previously described [12]. Briefly, users traced manually the main direction observed in one field of view as apparent by multiple parallel tracks in the different nuclei. The software automatically refined tracks in each nucleus based on this indication (Fig. 1D), by only considering tracks where there were at least 4 RIF. To consider the radial displacement of RIF (perpendicular to the track), as we previously described [12], a stripe of 1.2 µm width along each track was sampled for the maximum intensity in the direction perpendicular to the track. This led to one-dimensional intensity curve with maximal intensities along the track (lower panel, Fig. 1D). The imaging algorithm for 53BP1 RIF detection along these 1D profiles has already been described in our previous work [10 12 13]. The final result is a curve for the number of 53BP1 RIF/µm as a function of stage position and therefore as a function of LET (Fig. 1E). This was done for three different ions (Oxygen, Silicon and Iron) five min after exposure. The results show a clear saturation of RIF/µm around 200 keV/µm. It is interesting to note that the total intensity of 53BP1 signal within all RIF along each track increases linearly with LET (Fig. 1F – see material and method for details). This indicates that 53BP1 recruitment is proportional to the number of DSBs but the number of RIF is not, suggesting multiple DSBs may be present in the same RIF.

Modeling and validating DSB clustering model.

Evidence suggesting that RIF move over large distances in the nucleus has recently been reviewed [14]. From this body of work, we hypothesize that DSBs can merge into repair domains [13]. It has been shown that continuous streaks of RIF induced by high-LET alpha ions are quickly converted into isolated, large and bright RIF within minutes to hours after irradiation, suggesting the gathering of lesions into clusters [15]. More recently, we and others have shown that RIF quickly move into low DNA density regions [12 16] and that nuclear territory can lead to interrupted or deformed track patterns [17].

We introduce here a Monte Carlo method simulating DSB merging into RIF. We model breast cells as cylinders with a diameter of 7 µm and a height of 3 µm (Fig. 2A), based on the average shape observed using 3D microscopy. The nucleus is simulated as a 3D grid, using a pixel size of 0.1 µm. We assume a constant DSB yield (α) of 35 DSB/Gy for any radiation type. The probability of having one DSB in one pixel is therefore equal to α divided by the number of pixels within one nucleus and multiplied by the dose within this pixel. Microdosimetry for X-ray simulations is trivial and assumes equal doses in all pixels.

Two clustering mechanisms are investigated to see which model best matches the experimental RIF yield. The first clustering model (interaction model) assumes that DSBs sense each other and coalesce randomly via interaction forces. For this first assumption,

we use hierarchical clustering methods to decide which DSBs interact and form clusters. Agglomerative clustering is used, in which each DSB begins as its own cluster, and the two clusters with a minimum distance are joined iteratively. We tested three distance metrics to simulate different cost functions within the cell. In hierarchical clustering methods, the cost function is used to minimize distances between DSB. The average distance algorithm simply averages all distances between DSBs in one RIF with DSBs in another. The complete distance algorithm represents the DSBs that are furthest away from each other. Finally, Ward's distance method minimizes the within-cluster variance that results from clustering two RIFs [18]. One should note that Ward's distance does not directly translate to physical separation.
The second clustering model ("repair domain" model) that we tested assumes that the nucleus is divided into separate domains and any DSBs occurring within the same domain are merged into one single RIF. Both the interaction model and the "repair domain" model are illustrated in Fig. 2B.

Interaction distances or repair domain size are referred as the distance parameter for these various models. In order to determine the optimum distance parameter for each model, a parameter sweep was performed between 1 and 1.7 μm, with step increments of 0.05 μm. For each parameter value tested, 200 nuclei were simulated for each four doses of interest (0.25, 0.5, 1 and 2 Gy). RIF/cell were predicted as a function of dose and compared to values published by both Bedford and Costes lab on human breast MCF10A [13 19]. The root-mean-square error (RMSE) was computed for each parameter and the parameter with the smallest RMSE was kept as optimum (Fig. 2C). One can note that the "repair domain" model led to the lowest RMSE for a distance parameter of 1.5 μm. Fig. 2D shows the corresponding predicted dose response for the RIF yield (solid line), in comparison to published values.

Predicting high-LET RIF

As illustrated in Fig. 3A, HZE particles typically deposit part of their energy along linear tracks referred to as cores, while the remaining energy is deposited from electrons randomly outside the core (i.e. Delta-rays) scattered by Coulombic interaction with the particles, defining a region called the "penumbra". Microdosimetry is conducted as previously described [13]. Briefly, we assume a radial dose distribution decreasing as the distance square [20 21] from the track, and track positions are generated randomly (Fig. 3B). The number of tracks hitting each cell matches a Poisson distribution. The same geometry and grid system is used to simulate a nucleus as described in Fig. 2. Fig. 3A illustrates a simulation where an ion track hits a cylindrical cell right in the middle. The radius of the core is about ~10 nm for 1 GeV/n Fe ions whereas its penumbra radiate ~270 μm from the track [22 23]. For all ions considered, LET is computed using the relativistic Bethe formula, and half of the dose is assumed to go into the penumbra and formula for radial dependence is shown in Fig. 3B for both the core and penumbra regions.

Distance parameters obtained for the best fit of X-ray-induced foci obtained in Fig. 2C are applied to the very heterogeneous dose distribution of HZE across a wide range of ion energies and charges. Both the "interaction model" and the "repair domain" model are

used to predict the number of RIF per unit length one expects to observe using microscopy. Colored areas in graphs from Fig. 3C represent the average range of RIF/µm within one standard deviation, based on 200 nuclei simulations per LET point. By comparing these results with the experimental RIF linear dependence for all three ions presented in Fig. 1E, one can compute the relative error for each model and conclude that the "repair domain" model yields the best prediction across the LET range considered here, with an overall relative error of 12% against 28%, 18% and 28% for the average, complete and Ward clustering methods respectively.

Predicting cell survival RBE with DSB clustering

In this final section, we introduce a mathematical formalism predicting cell death as a function of both the number of DSB (classic target theory) and the number of DSB pairs clustered into one RIF (cluster theory). This can be expressed mathematically as followed:

$$P_{death} = 1 - e^{-\gamma(N + a \sum_{i=[2,N]} N_i C_2^i)} \quad (1)$$

Where N is the number of DSB generated by the exposure and is typically proportional to the dose ($N = \alpha D$), N_i is the number of RIF comprised of i DSBs as illustrated in Fig. 4A. γ and a are the survival parameters that can be fitted using experimental survival curves from X-ray. In this approach, we are assuming death is proportional to the number of DSB and to all potential rearrangements between two DSBs located within the same clusters (RIF). This later term is described in equation 1 as the variable C_2^i which represents the number of potential DSB pairs that can be formed out of a group of i DSBs. The concept behind this model is that DSB pairing increases the risk of chromosomal rearrangements (and thus death). Therefore, the more combination of DSB pairs in one cluster, the more likely chromosomal rearrangement will take place. In contrast, the generalized LEM model first evaluates the local equivalent X-ray dose that leads to the same number of isolated and clustered DSB for a given ion. The linear-quadratic dose dependence of X-ray for cell death is then computed for the equivalent dose to predict cell death [24].

X-ray survival curves in nonmalignant breast epithelial cells (MCF10A) were published by the Bedford group [19] and are used here to determine a and γ survival parameters. In this section, we only use the "repair domain" model for DSB clustering as it is the model that best fit both X-ray and HZE RIF dose dependence. The model was used to predict N and N_i as a function of X-ray dose. There are multiple solutions that lead to survival curves within the error bars of experimental data and higher doses for X-ray would be necessary to better describe dose curvature at very high doses. In order to test the maximum impact of the DSB pairing term on survival curves, we kept the fit with the highest γa parameter. This leads to γ=0.0040 and γa = 0.0072 and simulations of 200 nuclei per dose points are shown as a pink region overlapping experimental data point (Fig. 4B). This choice of parameter leads to a maximum differential between low and high-LET. More specifically, using the microdosimetry of HZE, new values for N and N_i are derived for individual nuclei exposed to a variety of ions (E=1,10,50,100,200,400,800,1600 MeV/n; Z=6,8,10,14,18,22,26; 500 nuclei simulated in

group of 50 nuclei for each E and Z). Predictions for one set of 50 nuclei are shown in Fig. 4C as red circles and compared to the X-ray experimental survival. Predictions are fitted with an exponential fit (red dotted line) and HZE dose equivalent for 10% survival is computed. RBE is then computed by taking the ratio of the 10% survival X-ray dose (i.e. 4 Gy) with the predicted HZE equivalent dose. Average RBE for all 10 repeats for each E and Z simulated values are shown as a function of LET in Fig. 4D. RBE predictions for MCF10A increases with LET reaching a maximum of 3 at ~500 keV/µm, after which the RBE decreases with LET.

DISCUSSION

RIF clustering has been observed in many independent studies [12 15 16 25-29], and its meaning and consequences remain mostly speculative. As previously suggested [30 31], such a mechanism would be an efficient and physiological way to deal with lesions in the very low dose range (mGy) as the majority of the lesions would remain isolated into one repair domain. On the other hand, at higher doses or along high-LET tracks, DSBs clustering could increase risk of translocations and cell death, as recently reviewed [14]. For example, DSB clustering in human white blood cells has been proposed as a mechanism for chromosomal rearrangements observed after exposure to densely ionizing radiation [32]. We test here two potential mechanisms for DSB clustering. The interaction model assumes that RIF formation and DSB clustering reflect a combination of adherent properties of various repair proteins leading to an interaction force and random coalescence. The "repair domain" model assumes that the nucleus is separated into sub-nuclear regions for repair and that DSB generated in the same repair domain can merge into one single RIF.

Our simulations suggest the "repair domain" hypothesis is able to best explain the reduction in the number of RIF/Gy observed for increasing X-ray doses that we [13] and others [19] have previously published on for studies with non-malignant human breast cell line MCF10A. In addition, novel data presented here on the LET dependence of RIF in MCF10A are again better explained with the "repair domain" model. Confirming the accuracy of our approach, both our work here and previous work [33] done on adherent human cells exposed to increasingly higher local doses of ions (LET ranging from 150 to 14,300 keV/µm), show that RIF linear yield along high-LET track reaches a maximum of ~1 RIF/µm along individual ion tracks. Our DSB clustering model suggests that repair domain would have an average diameter of ~1.55 µm. This length is in good agreement with the theoretical distances at which two DSBs trigger chromosomal rearrangements [34 35]. On the other hand, this length is three times larger than the theoretical voxel size of 0.54 µm reported in the LEM model. The LEM voxel size is derived by doing a parameter sweep leading to the best RBE predictions across a wide range of ions [24]. In contrast, the domain size we report reflects observable repair processes in the nucleus. Domain size discrepancies may also reflect a different nuclear organization between the various cell lines. For example, MCF10A may have fewer repair domains leading to more clustering and larger apparent domains. In addition, cell survival is predicted differently in both models and will contribute to further discrepancies.

We recently reported that clustered RIF are more persistent than isolated RIF [14], suggesting that DSBs associated with RIF clusters are more difficult to repair. In agreement, the LEM model assumes that DSBs in close proximity have a higher probability of inducing cell death than isolated DSBs [36 37]. Experimental radiation survival curves can be fitted accurately with the LEM model if one assumes that two DSBs located in one 'Giant Loop' have a higher probability of inducing cell death than two DSBs on distinct Giant Loops [38]. 'Giant Loop' here refers to a large chromatin region that spans several megabases [39 40]. Similarly, our cell death model hypothesizes that one can derive the probability of death based on all DSBs and on the number of potential DSB pairing within each DSB clusters. The downward curvature observed at high doses of X-ray reflects the additional death generated by the increasing number of DSBs within one RIF. This can be predicted without using the linear-quadratic dose dependence from X-ray as done with the LEM model.

In conclusion, our approach gives an independent validation of the generalization of the LEM principles recently introduced [24], where cell death is derived by simply predicting isolated and clustered DSBs. For many years, our community has been focusing on complex DSBs generated by HZE which are believed to be more difficult to repair accurately, leading to more cell death and mutations [41]. In contrast, our approach shows that DSB movements across microns in the nucleus may in fact be another essential cause of high RBE observed with energetic ions. Even though the RBE values we predict here for MCF10A have not been measured yet, they are in excellent agreement with similar studies. For example, the reported RBE for clonogenic survival of ~2 in primary breast cells exposed to 1 GeV/n Fe ions [4] is very close to the predicted RBE of 1.74 for the immortalized MCF10A line exposed to the same ion and energy. Finally, the shape of RBE for survival predicted here matches well the overkill effect observed in the upper hundreds of keV/µm, but the peak is at a higher LET value than previously reported [42]. Future work will focus on validating this approach to other cell lines and to test how cell cycle and DNA repair defects interface in this model.

More generally, by having a mechanism-based model for DSB clustering and by modeling how it impacts cell death, one can predict the response of human cells for dose regimens that are difficult to measure experimentally due to too small differences. Classically, X-ray survival is interpreted by the linear-quadratic model and low dose response are inferred from this formalism. In contrast, DSB pairing will be minimum at very low dose ranges (mGy and less), suggesting simpler and more accurate DNA repair for ambient and occupational radiation exposures. The current usage of the linear-no-threshold (LNT) model for cancer risk assessment from ionizing radiation currently assumes linear risk from Gy to mGy[43]. LNT should therefore be reconsidered in favor of more accurate models that take into account non-linear processes such as DSB pairing dose dependence.

MATERIAL AND METHODS

Cell culture: Human mammary epithelial cells, MCF10A obtained from ATCC, were grown in MEMB media supplemented with bovine pituitatry hormone (13mg/ml), hydrocortisone (0.5mg/ml), hEGF (10µg/ml), insulin (5mg/ml) and cholera toxin

(100ng/ml) (Invitrogen Inc., Carlsbad, CA). MCF10A were cultivated at 37°C, with 95% humidity and 5% CO_2. Cells were seeded in Permanox plastic 8-well Lab-Tek chamber slides (Nalge Nunc International Corp., Rochester, NY). The cells were cultivated until they formed a monolayer (~85% confluent) prior to irradiation. High LET radiation was done at the NASA Space Radiation Laboratory of the Brookhaven National Laboratory.

Reagents: Primary: mouse monoclonal anti phospho-histone H2AX (Ser139) antibody (Lot # 27505; Upstate Cell Signaling Solutions Inc. Charlottesville, VA) used at 1.42 μg/ml; rabbit polyclonal anti 53BP1 (Lot # A300-272A, Bethyl Lab, Montgomery, TX) used at 5 μg/ml. Secondary antibodies were used at 1:300 (Dk anti-Rb Alexa 594, Lot# 40247A, and Gt anti-Ms Alexa 488, lot A11029 from Molecular Probes, Invitrogen, Carlsbad, CA).

Immunofluorescence: Chambers were fixed at room temperature for 15 min using 2% paraformaldehyde followed by successive wash and permeabilization with 100% methanol for 20 min at -20ºC. Non-specific sites were blocked using 1% BSA for 90 minutes. The cells were incubated two hours at room temperature with primary antibodies in blocking buffer in a humidified chamber. Following washes, primary antibody binding was detected using species appropriate fluorochrome labeled secondary antibodies incubated for 1 hour at room temperature. Nuclei were counterstained with DAPI (4',6-Diamidino-2-Phenylindole) using 0.5 μg/ml. Slides were mounted in Vectashield (Vector Laboratories Inc., Burlingame, CA) and stored at -20°C until evaluated.

Image analysis and computer modeling: Cells were viewed and imaged using a Zeiss Axiovert epifluorescence microscope (Carl Zeiss, Jena, Germany) equipped with a multiband pass filter and a differential wavelength filter wheel. Images were acquired using a Zeiss plan-apochromat 40X dry, with a NA of 0.95 and a scientific-grade 12-bit charged coupled device camera (Axiocam). All images were captured with the same exposure time so that intensities were within the 12-bit linear range. All image manipulation and analysis were done with Matlab (MathWorks, Inc., Natick, MA) and DIPimage (image processing toolbox for Matlab, Delft University of Technology, The Netherlands). Method for foci detection and ion track detection were previously described [13]. In order to visualize the amount of protein recruitment along track per unit length, foci mask along track was used to integrate the full pixel intensity of 53BP1 and by dividing by the length of the track. Because exposure times for image acquisition of 53BP1 signal for different ions were different, we normalized the computed track intensity by dividing it with the minimum average intensity per unit length detected for each LET. This typically led to the first measurement of intensity to be 1 at the entry point. To visualize the dependence with LET, we then multiplied each normalized curve by the value of the LET at the entry of the slides. This led to 1:1 ratio between normalized intensity and LET (see Fig. 1F). Microdosimetry and cell simulation were done in Matlab as well, by taking advantage of the 3D imaging capability of DIPImage. Cells were defined as 3D binary masks.

ACKNOWLEDGEMENTS

The authors would like to thank Dr. Jasmina Vujic, Dr. Bethany Goldblum and Nicholas Brickner from the nuclear engineering department at UC Berkeley for their initial contribution on microdosimetry. SVC, WG, TD, JT are supported by NASA Specialized Center for Research in Radiation Health Effects [NNJ09HC64I] and the Low Dose Scientific Focus Area, United States Department of Energy [DE-AC02-05CH11231]. NV is supported by the National Space Biomedical Research Institute.

Disclaimer

REFERENCES

1. Barratt MR, Pool SL. *Principles of clinical medicine for space flight*. New York: Springer, 2008.
2. Sinclair WK, Gunter SE, Cole A. The relative biological effectiveness of 200-kvp x-rays, cobalt-60 gamma-rays, and 22-Mevp x-ray, determined from the dose-survival curve of Saccharomyces cerevisiae. Radiation research 1959;**10**(4):418-32
3. Alpen EL, Powers-Risius P, Curtis SB, et al. Tumorigenic potential of high-Z, high-LET charged-particle radiations. Radiation research 1993;**136**(3):382-91
4. Andarawewa KL, Costes SV, Fernandez-Garcia I, et al. Lack of radiation dose or quality dependence of epithelial-to-mesenchymal transition (EMT) mediated by transforming growth factor beta. Int J Radiat Oncol Biol Phys 2011;**79**(5):1523-31 doi: S0360-3016(10)03682-5 [pii]
10.1016/j.ijrobp.2010.11.058[published Online First: Epub Date]|.
5. Ritter S, Durante M. Heavy-ion induced chromosomal aberrations: a review. Mutation research 2010;**701**(1):38-46 doi: 10.1016/j.mrgentox.2010.04.007[published Online First: Epub Date]|.
6. Goodhead DT. Mechanisms for the biological effectiveness of high-LET radiations. Journal of radiation research 1999;**40 Suppl**:1-13
7. Cucinotta FA, Durante M. Cancer risk from exposure to galactic cosmic rays: implications for space exploration by human beings. Lancet Oncol 2006;**7**(5):431-5
8. Douglas BG, Fowler JF. The effect of multiple small doses of x rays on skin reactions in the mouse and a basic interpretation. Radiation research 1976;**66**(2):401-26
9. Scholz M, Kellerer AM, Kraft-Weyrather W, et al. Computation of cell survival in heavy ion beams for therapy. The model and its approximation. Radiation and environmental biophysics 1997;**36**(1):59-66
10. Costes SV, Boissiere A, Ravani S, et al. Imaging features that discriminate between foci induced by high- and low-LET radiation in human fibroblasts. Radiation research 2006;**165**(5):505-15

11. Ziegler JF, Biersack JP, Littmark U. *The stopping and range of ions in solids*. Oxford: Pergamon Press, 1985.
12. Costes SV, Ponomarev A, Chen JL, et al. Image-based modeling reveals dynamic redistribution of DNA damage into nuclear sub-domains. PLoS Comput Biol 2007;**3**(8):e155 doi: 10.1371/journal.pcbi.0030155[published Online First: Epub Date]|.
13. Neumaier T, Swenson J, Pham C, et al. Evidence for formation of DNA repair centers and dose-response nonlinearity in human cells. Proc Natl Acad Sci U S A 2012;**109**(2):443-8 doi: 1117849108 [pii]
10.1073/pnas.1117849108[published Online First: Epub Date]|.
14. Chiolo I, Tang J, Georgescu W, et al. Nuclear dynamics of radiation-induced foci in euchromatin and heterochromatin. Mutation research 2013 doi: 10.1016/j.mrfmmm.2013.08.001[published Online First: Epub Date]|.
15. Aten JA, Stap J, Krawczyk PM, et al. Dynamics of DNA double-strand breaks revealed by clustering of damaged chromosome domains. Science 2004;**303**(5654):92-5
16. Chiolo I, Minoda A, Colmenares SU, et al. Double-strand breaks in heterochromatin move outside of a dynamic HP1a domain to complete recombinational repair. Cell 2011;**144**(5):732-44 doi: 10.1016/j.cell.2011.02.012[published Online First: Epub Date]|.
17. Jakob B, Splinter J, Conrad S, et al. DNA double-strand breaks in heterochromatin elicit fast repair protein recruitment, histone H2AX phosphorylation and relocation to euchromatin. Nucleic Acids Res 2011 doi: 10.1093/nar/gkr230[published Online First: Epub Date]|.
18. Ward JH, Jr. Hierarchical Grouping to Optimize an Objective Function. Journal of the American Statistical Association 1963;**58**(301):236-44
19. Lin YF, Nagasawa H, Peng Y, et al. Comparison of several radiation effects in human MCF10A mammary epithelial cells cultured as 2D monolayers or 3D acinar stuctures in matrigel. Radiation research 2009;**171**(6):708-15 doi: 10.1667/RR1554.1[published Online First: Epub Date]|.
20. Chatterjee A, Maccabee HD, Tobias CA. Radial cutoff LET and radial cutoff dose calculations for heavy charged particles in water. Radiation research 1973;**54**(3):479-94
21. Tobias CA, Lyman JT, Chatterjee A, et al. Radiological physics characteristics of the extracted heavy ion beams of the bevatron. Science 1971;**174**(14):1131-4
22. Costes S, Streuli CH, Barcellos-Hoff MH. Quantitative image analysis of laminin immunoreactivity in skin basement membrane irradiated with 1 GeV/nucleon iron particles. Radiation research 2000;**154**(4):389-97
23. Magee JL, Chatterjee A. Radiation chemistry of heavy-particle tracks. 1. General considerations. J. Phys. Chem. 1980;**84**:3529-36
24. Elsasser T, Weyrather WK, Friedrich T, et al. Quantification of the relative biological effectiveness for ion beam radiotherapy: direct experimental comparison of proton and carbon ion beams and a novel approach for treatment planning. Int J Radiat Oncol Biol Phys 2010;**78**(4):1177-83 doi: 10.1016/j.ijrobp.2010.05.014[published Online First: Epub Date]|.

25. Kruhlak MJ, Celeste A, Dellaire G, et al. Changes in chromatin structure and mobility in living cells at sites of DNA double-strand breaks. J. Cell Biol. 2006;**172**(6):823-34
26. Krawczyk PM, Stap J, van Oven C, et al. Clustering of double strand break-containing chromosome domains is not inhibited by inactivation of major repair proteins. Radiat Prot Dosimetry 2006;**122**(1-4):150-3 doi: 10.1093/rpd/ncl479[published Online First: Epub Date]|.
27. Falk M, Lukasova E, Gabrielova B, et al. Chromatin dynamics during DSB repair. Biochim Biophys Acta 2007;**1773**(10):1534-45 doi: 10.1016/j.bbamcr.2007.07.002[published Online First: Epub Date]|.
28. Jakob B, Splinter J, Durante M, et al. Live cell microscopy analysis of radiation-induced DNA double-strand break motion. Proc Natl Acad Sci U S A 2009;**106**(9):3172-7 doi: 10.1073/pnas.0810987106[published Online First: Epub Date]|.
29. Krawczyk PM, Borovski T, Stap J, et al. Chromatin mobility is increased at sites of DNA double-strand breaks. J Cell Sci 2012;**125**(Pt 9):2127-33 doi: 10.1242/jcs.089847[published Online First: Epub Date]|.
30. Savage JR. Insight into sites. Mutation research 1996;**366**(2):81-95
31. Savage JR. Reflections and meditations upon complex chromosomal exchanges. Mutation research 2002;**512**(2-3):93-109
32. Anderson RM, Stevens DL, Goodhead DT. M-FISH analysis shows that complex chromosome aberrations induced by alpha -particle tracks are cumulative products of localized rearrangements. Proc Natl Acad Sci U S A 2002;**99**(19):12167-72 doi: 10.1073/pnas.182426799[published Online First: Epub Date]|.
33. Jakob B, Splinter J, Taucher-Scholz G. Positional stability of damaged chromatin domains along radiation tracks in mammalian cells. Radiation research 2009;**171**(4):405-18 doi: 10.1667/RR1520.1[published Online First: Epub Date]|.
34. Sachs RK, Chen AM, Brenner DJ. Review: proximity effects in the production of chromosome aberrations by ionizing radiation. Int J Radiat Biol 1997;**71**(1):1-19
35. Sachs RK, Ponomarev AL, Hahnfeldt P, et al. Locations of radiation-produced DNA double strand breaks along chromosomes: a stochastic cluster process formalism. Math Biosci 1999;**159**(2):165-87
36. Friedrich T, Scholz U, Elsasser T, et al. Systematic analysis of RBE and related quantities using a database of cell survival experiments with ion beam irradiation. Journal of radiation research 2012 doi: 10.1093/jrr/rrs114[published Online First: Epub Date]|.
37. Grun R, Friedrich T, Elsasser T, et al. Impact of enhancements in the local effect model (LEM) on the predicted RBE-weighted target dose distribution in carbon ion therapy. Phys Med Biol 2012;**57**(22):7261-74 doi: 10.1088/0031-9155/57/22/7261[published Online First: Epub Date]|.
38. Friedrich T, Durante M, Scholz M. Modeling cell survival after photon irradiation based on double-strand break clustering in megabase pair chromatin loops. Radiation research 2012;**178**(5):385-94 doi: 10.1667/RR2964.1[published Online First: Epub Date]|.

39. Yokota H, van den Engh G, Hearst JE, et al. Evidence for the organization of chromatin in megabase pair-sized loops arranged along a random walk path in the human G0/G1 interphase nucleus. J Cell Biol 1995;**130**(6):1239-49
40. Sachs RK, van den Engh G, Trask B, et al. A random-walk/giant-loop model for interphase chromosomes. Proc Natl Acad Sci U S A 1995;**92**(7):2710-4
41. Pastwa E, Neumann RD, Mezhevaya K, et al. Repair of radiation-induced DNA double-strand breaks is dependent upon radiation quality and the structural complexity of double-strand breaks. Radiation research 2003;**159**(2):251-61
42. Blakely EA, Tobias CA, Yang TC, et al. Inactivation of human kidney cells by high-energy monoenergetic heavy-ion beams. Radiation research 1979;**80**(1):122-60
43. Brenner DJ, Doll R, Goodhead DT, et al. Cancer risks attributable to low doses of ionizing radiation: assessing what we really know. Proc Natl Acad Sci U S A 2003;**100**(24):13761-6

FIGURE LEGEND

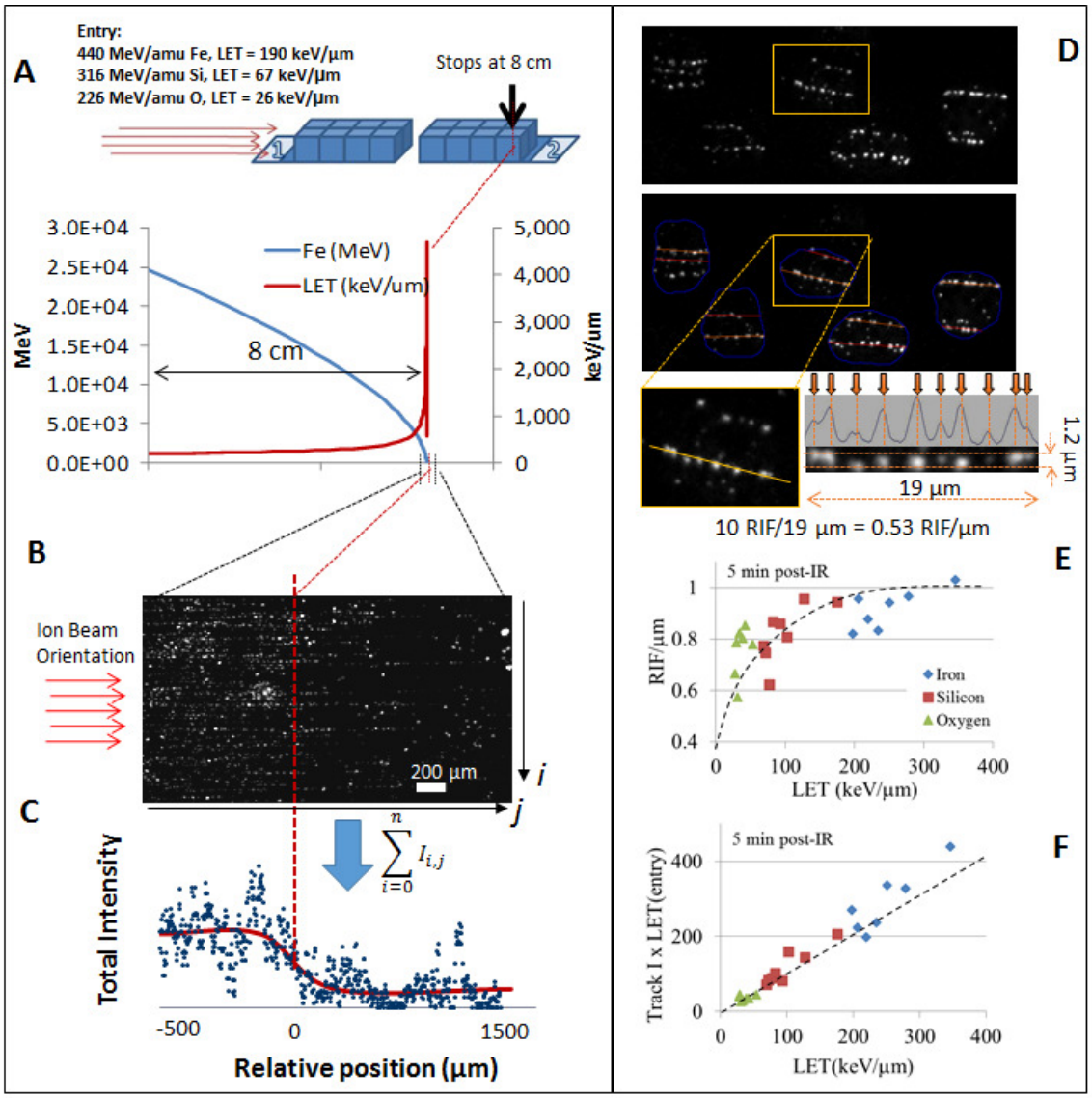

Figure 1. Experimental protocol. (A) Schematic showing the slide arrangement for ions to traverse 8 cm of MCF10A grown as confluent monolayer. Stage position allows the theoretical computation of the energy and LET as illustrated in the graph for Fe ion. **(B)** Visualization of 8 cm point in the slides where the particle is expected to stop, using γH2AX labeling. **(C)** By summing the amount of signal along the *i* axis in (B), one can visualized the drop of DNA damage, once the particle has stopped at position 0 (0 represents the expected stopping point of the ion). **(D)** Illustration of image algorithm used to detect individual tracks. Software automatically identifies tracks (colored lines overlapping 53BP1 RIF in gray image). Intensity profiles are determined by summing the signal perpendicular to tracks with a 1.2 µm diameter so that local maxima can be more easily detected. This allows the computation of the number of RIF/µm. **(E)** Experimental RIF/µm measured for the three ions of interest here (Fe with Z=26, Si with Z=14 and O with Z=8). Dashed line helps visualize saturation of response with LET. **(F)** The normalized total intensity of 53BP1 detected in all RIF along tracks per unit length (see material and method for details) is proportional to LET as indicated by the dashed-line.

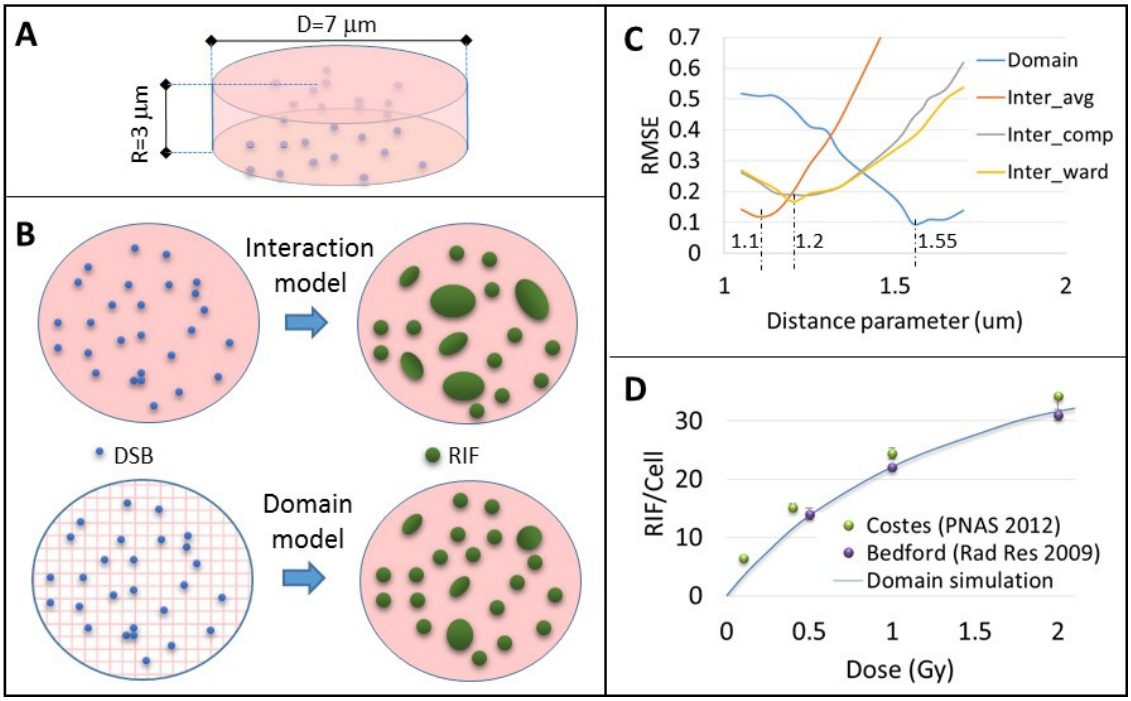

Figure 2. DSB clustering model and RIF predictions for X-rays. (A) Nucleus is modeled as a cylinder where DSB (blue spheres) are randomly generated using Monte Carlo methods. **(B)** Two clustering models are considered to produce RIF (green domains). The "interaction model" assumes neighboring DSB interact based on their inter-distance and a hierarchical clustering algorithm (three norms are used to compute distances: average, complete and Ward). The "repair domain" model assumes the nucleus is divided into cubical repair domains. Any DSBs within the same domain form one single RIF. **(C)** Sweeping the parameter values, we determine the optimum interaction distance to fit the X-ray RIF dose dependence for each model. **(D)** Best-fit simulations compared to experimental data.

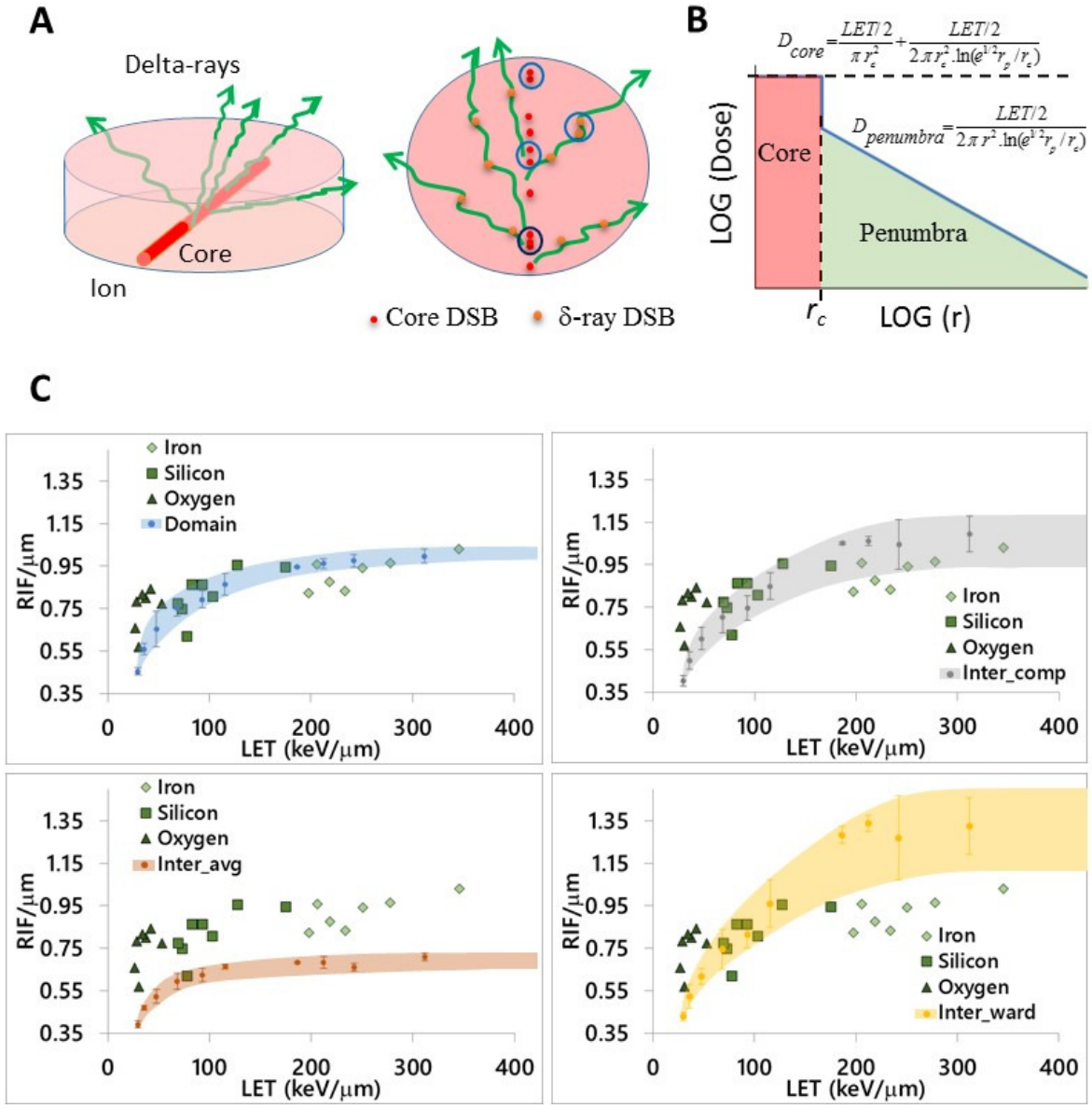

Figure 3. Predicting high-LET RIF. (A) Model schematic illustrating preferential formation of DSBs along the ion track. A small red cylinder crossing the nucleus in the middle along its length indicates the core of the HZE. Delta-rays generated in the core via Coulomb interactions are depicted as green arrows, depositing energy uniformly in a region called penumbra and generating DSB randomly in space. **(B)** Assumption and equation used for the radial profile of energy deposition ($1/r^2$ dependency based on Chatterjee's model) [20 21], where r, r_c, r_p are the radial distance from the track, the radius of the core and of the penumbra, respectively. **(C)** Prediction and experimental values of HZE RIF/μm based on clustering model. Results from the "repair domain" model, and the "interaction model" using the average, complete and Ward criteria are shown for distance parameters found to be optimum for X-ray data; they equal 1.55, 1.1, 1.2 and 1.2 μm respectively.

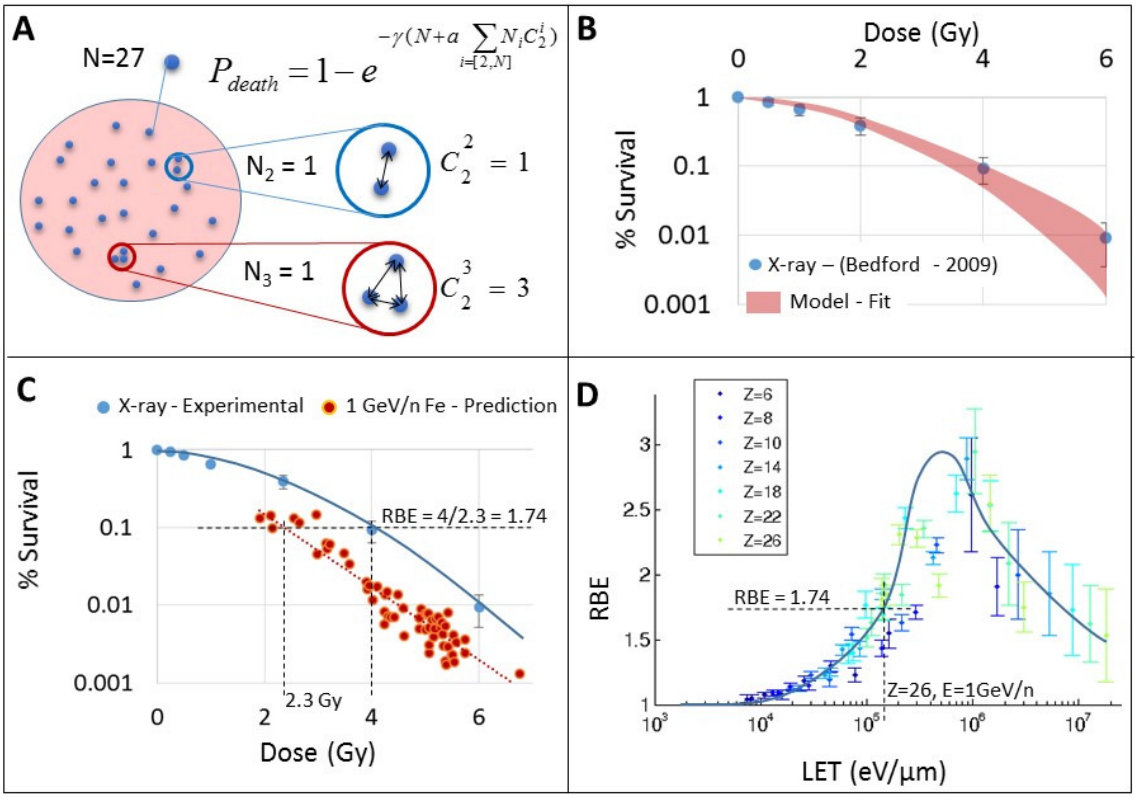

Figure 4. DSB clustering to predict cell death. (A) Our survival model assumes clustered DSB have additional impact on cell death. The red and blue circles indicate two clusters with 3 and 2 DSB in each respectively. For each cluster, the number of potential rearrangements between two DSBs is computed as the combinatorial of 2 with i components. If i=2 (blue circle cluster), there is only one combination ($C_2^2 = 1$). If i=3 (red circle cluster), there are three possible combinations ($C_2^3 = 3$). The equation for the probability of death shows an exponential with coefficient proportional to the number of all DSBs (N – classic term) and the total number of potential pairs of DSB formed in all clusters. **(B)** Best fit of X-ray survival data for MCF10A (γ=0.0040, γa = 0.0072). **(C)** Using X-ray parameters we can predict cell survival (each red point is one cell simulation) exposed to a hypothetical 1 GeV/n Fe ion. Relative biological effectiveness (RBE) is computed for the 10% survival endpoint. **(D)** RBE prediction for a large array of ions (Z of each ion indicated in legend) based on the same model parameters.

DISCLAIMER